Journal of Statistical Physics, Vol. 68, Nos. 3/4, 1992

Lattice Gas Simulations of Osmosis

E. G. Flekkøy,[1] J. Feder,[1] and T. Jøssang[1]

An analysis of the phenomenon of osmosis within the lattice gas model is presented. The model considered is a two-species version of the Frisch–Hasslacher–Pomeau model with rest particles and a semipermeable membrane which is implemented as a boundary that blocks one species, but lets the other pass freely. In this way the equilibrium between a pure and a mixed subsystem can be studied. Analytic expressions for both the pressure difference and the fluctuations of this quantity are obtained from the entropy function for the lattice gas, and we find that these results are in good agreement with those obtained from simulation. The osmotic flow across the membrane is also studied. We characterize the concentration boundary layer, and an analytic expression for the osmotic permeability as a function of porosity is compared with results from simulations.

KEY WORDS: Lattice gases; cellular automata; osmosis.

1. INTRODUCTION

Since the lattice gas model for the simulation of two- and three-dimensional fluid flow was introduced by Frisch, Hasslacher, and Pomeau (FHP)[1] a series of applications of the model have appeared. These include extensions of the model to several particle species for the simulation of diffusion phenomena[2] and models with surfaces tension for simulation of immiscible two-phase flow.[3–5] The flow of one particle species across a porous membrane has also been done. To our knowledge the present application to the phenomenon of osmosis is the first ever done.

For the phenomenon of osmosis to occur there must be a semipermeable membrane separating solutions of different concentrations and being impermeable to the solute. The solvent, being able to pass through the membrane, will tend to flow toward the side of higher concentration,

[1] Department of Physics, University of Oslo, Blindern, 0316 Oslo, Norway.

0022-4715/92/0800-0515$06.50/0

thereby diluting the solution on this side. In the case of no hydrostatic pressure difference across the membrane this process will lead to a steady flow of solvent. In the case of a closed system divided by a membrane the process of osmosis will support an equilibrium pressure difference across the membrane maximizing the entropy of the mixture.

Osmosis is a central mechanism in many biological processes. It occurs not only across the membranes of living cells, but also as a mechanism of transport into and out of organs in the body, such as kidney tubulus, the intestines, and blood capillaries, where also the hydrostatic pressure difference is important.

There exist many problems where the effects of hydrodynamic flow and osmosis combine.[7,8] The lattice gas automata (LGA) seem particularly well suited for this type of application: It has hydrodynamic behavior and, since it is a perticle-based model, it supports a natural definition of entropy and chemical potential. This is true also for the lattice Boltzmann model[9,10] and for the lattice BGK model recently introduced by Qian *et al.*[11] We start out, however, isolating the effect of osmosis, i.e., we focus on the equilibrium situation where osmosis supports a hydrostatic pressure difference, and where there is no flow. We calculate this pressure difference (or rather density difference) and the fluctuations in this quantity from the entropy function for the lattice gas. These results are then compared with those of simulation. These calculations provide a simple example of how concepts of equilibrium statistical mechanics can be employed within the framework of the lattice gas model.

Finally, we study the osmotic flow perpendicular to the membrane. In this case the system is not in equilibrium. We calculate the osmotic permeability of the membrane using an assumption of local equilibrium, and compare the theoretical result with the results of simulation.

2. OSMOTIC PRESSURE

We use a lattice as shown in Fig. 1, divided into two parts by a semipermeable wall that blocks red particles, but lets blue particles through. For every time step, particles first collide at the lattice sites and then propagate to a nearest neighbor site.

The lattice gas model we have chosen is a two-color version of the FHP-III model.[12] At each site there can be at most seven particles distributed over the seven available velocities (cells) $\mathbf{c}_i$, where $\mathbf{c}_0 = 0$ and $\mathbf{c}_1$ through $\mathbf{c}_6$ are the unit vectors connecting neighboring sites on the lattice. The vector $\mathbf{c}_1$ points downward to the right and the other $\mathbf{c}_i$ are labeled counterclockwise. The configuration at a site $\mathbf{x}$ is denoted $s(\mathbf{x}) = (r(\mathbf{x}), b(\mathbf{x}))$, where $r = \{r_i, i = 0,..., 6\}$ and $b = \{b_i, i = 0,..., 6\}$ and r_i

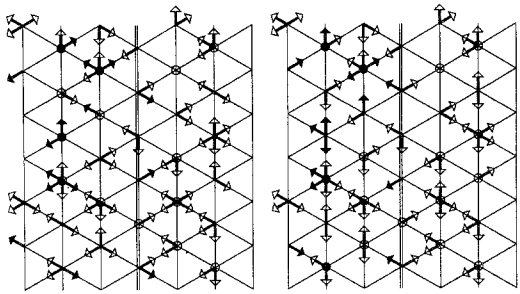

Fig. 1. The state of the lattice before and after collisions. Red particles are represented by solid arrows and circles, while blue particles are represented by open symbols. The membrane collisions are implemented along the vertical midline of the lattice reflecting red particles 180 deg. The red particles are therefore confined to the left of this midline.

(b_i) is a Boolean variable indicating the presence of a red (blue) particle with velocity $\mathbf{c}_i$. The variables r_i and b_i cannot simultaneously equal one.

In this model where particles are either at rest or move with unit velocity, the equation of state is has no temperature dependence, and has the simple form[12]

$$p = \tfrac{3}{7}\rho \tag{1}$$

where p is the pressure and ρ is the site density of particles.

The interparticle collision rules are such that all output configurations having the same number of red and blue particles and the same momentum as the input configuration are chosen with the same probability. The collision rules therefore satisfy the condition

$$\sum_s A(s \to s') = 1 \qquad \text{for all} \quad s' \tag{2}$$

which is known as semi-detailed balance. $A(s \to s')$ is the probability that a collision brings the configuration s into s' (in fact, the collision rules also satisfy detailed balance).

In addition to conserving color and linear momentum, the collisions also conserve the unphysical staggered momentum.[13–15] The particle–wall collisions, however, conserve neither staggered nor linear momentum, so the only quantities that are conserved globally are the numbers of red and blue particles.

The conservation laws and the semi-detailed balance form the entire basis for the statistical analysis which follows. Conservation of the total amounts of both red and blue particles means that only states [a state is given by the set of all the configurations $s(\mathbf{x})$ on the lattice] with the given

amounts of red and blue will be available for the lattice gas in the course of time, while semi-detailed balance means that if every such state is equally probable at the time t, this will also be the case at the time $t+1$. A time step includes both the propagation step and the collision step.

Assuming therefore that the equilibrium situation is adequately described by an ensemble where every state having the given total amounts of red (R) and blue (B) is equally represented, every state is equally probable. The probability $P(r_i, b_i)$ for the occupation numbers (r_i, b_i) at a given cell is then simply proportional to the number of states $\Omega(R-r_i, B-b_i)$ available to the rest of the system:

$$P(r_i, b_i) \sim \Omega(R-r_i, B-b_i) \tag{3}$$

Note that since the equilibrium state is homogeneous, $P(r_i, b_i)$ is position independent. The entropy S of the gas as a whole is defined as

$$S = \ln \Omega \tag{4}$$

and the chemical potentials μ_r and μ_b are defined as

$$\mu_r = -\frac{\partial S}{\partial R}, \qquad \mu_b = -\frac{\partial S}{\partial B} \tag{5}$$

The entropy defined above is (apart from a sign and a constant term) identical to the equilibrium value of the information measure introduced by Hénon.[16] This can be shown by actually counting the states available to the system. By taking the logarithm of Eq. (3), carrying out a Taylor expansion to first order in r_i and b_i, and normalizing, we find that

$$P(r_i, b_i) = z^{-1} e^{\mu_r r_i + \mu_b b_i} \tag{6}$$

where z is the one-particle partition function

$$z = \sum_{r_i, b_i}{}' e^{\mu_r r_i + \mu_b b_i} \tag{7}$$

The prime on the summation symbol indicates that the term with $r_i = b_i = 1$ is not included in the summation. The chemical potentials are easily expressed by the average number of red and blue particles per cell using the relations

$$d_r = \sum_{r_i, b_i}{}' r_i P(r_i, b_i) \tag{8}$$

$$d_b = \sum_{r_i, b_i}{}' b_i P(r_i, b_i) \tag{9}$$

This gives

$$\mu_r = \ln \frac{1-d}{d_r}$$
$$\mu_b = \ln \frac{1-d}{d_b} \tag{10}$$

where $d = d_r + d_b \in [0, 1]$ is the total density per cell.

Having obtained the dependence of the equilibrium distribution on the chemical potentials, we now turn to the computation of the osmotic pressure. At equilibrium the color will be distributed in such a way that the total entropy is maximized. In the case where a semipermeable wall allows only blue particles to move freely, this means that the equilibrium condition between the two parts of the lattice (numbered 1 and 2) is given by

$$\mu_{b1} = \mu_{b2} \tag{11}$$

This equilibrium condition can then be written in the form

$$\frac{1-d_1}{d_{b1}} = \frac{1-d_2}{d_{b2}} \tag{12}$$

We did not have to determine the entropy S in order to write down this equation. By rewriting Eq. (12) as

$$(1-d_1)\, d_{b2} = (1-d_2)\, d_{b1} \tag{13}$$

it is recognized as the condition that the probability of a blue particle crossing the semipermeable wall from left to right must equal the probability of crossing in the other direction. (The probability of having a particle pass the wall from a given cell is the probability of having a particle at that cell times the probability of having a vacant cell at the other side.)

Defining the average blue density as $d_b = \frac{1}{2}(d_{b1} + d_{b2})$, we obtain from Eq. (12) the density difference

$$\Delta d = d_1 - d_2 = \left(1 - \frac{2d_b}{2-d_r}\right) d_r \tag{14}$$

In Fig. 2, Δd is shown as a function of d_r. Two conflicting effects come into play: The effect of the maximization of the entropy tends to increase the density difference and the effect of the exclusion principle tends to decrease it. Without the exclusion principle Δd would be a linear function of d_r, while Fig. 2 shows curves falling off from linear behavior with increasing densities.

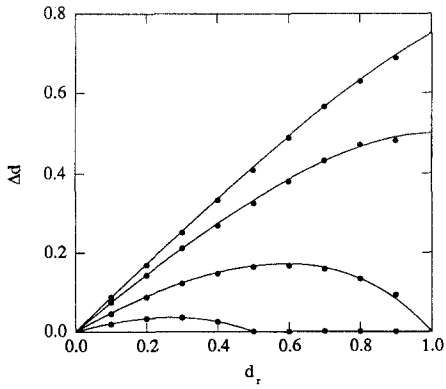

Fig. 2. The density difference Δd as a function of the density of red d_r in the left part of the lattice (see Fig. 1). The solid curves give the theoretical result [Eq. (14)] while the dots give the simulation values obtained by time averaging over 4000 time steps. The average blue density d_b has the values 1/8, 1/4, 1/2, and 3/4 from top to bottom.

The simulations were carried out on a 100×50 lattice and the densities were averaged over 4000 time steps after the system had reached equilibrium.

The system was initialized with values of the densities different from the equilibrium values by choosing the density of blue in the mixed part as low as possible. The approach to equilibrium is then a two-step process: First a sound wave, caused by the free expansion of the blue particles into the mixed area of lower density, evens out the pressure difference between the two parts. On the 100×50 lattice used this wave typically equilibrates by 200 time steps. Then the red and blue components start to mix. Being controlled by diffusion, this process is much slower, taking approximately 3000 time steps to reach equilibrium.

We turn now to the calculation of the fluctuation in the density difference. Since there are no variations in the density of red d_r, variations in the density difference $\delta(\Delta d)$ are caused solely by variations in the blue densities,

$$\delta(\Delta d) = \delta d_{b1} - \delta d_{b2} \tag{15}$$

But since the total number of blue particles is conserved,

$$\delta d_{b2} = -\delta d_{b1} \tag{16}$$

the mean square fluctuation in the density difference can be written

$$\langle \delta^2(\Delta d) \rangle = 4 \langle \delta^2 d_{b1} \rangle \tag{17}$$

Due to semi-detailed balance the probability P of finding the system with a certain value of a given parameter, in this case d_{b1}, is proportional to the number of states available to the system for that particular value:

$$P(d_{b1}) \sim \Omega(d_{b1}) = e^{S(d_{b1})} \tag{18}$$

Normalization then gives

$$P(d_{b1}) = P(\bar{d}_{b1})\, e^{-\Delta S} \tag{19}$$

where we have defined the increment ΔS as

$$\Delta S = S(d_{b1}) - S(\bar{d}_{b1}) \approx -\frac{1}{2}\frac{\partial^2 S}{\partial d_{b1}^2}(d_{b1} - \bar{d}_{b1})^2 \tag{20}$$

Thus the probability function $P(d_{b1})$ is Gaussian and the mean square fluctuation is therefore

$$\delta^2 d_{b1} = -\left(\frac{\partial^2 S}{\partial d_{b1}^2}\right)^{-1} \tag{21}$$

The derivatives are evaluated at the mean value $d_{b1} = \bar{d}_{b1}$. Again it is actually not required to count the number of states, since

$$\frac{\partial^2 S}{\partial d_{b1}^2} = \frac{\partial^2 S_1}{\partial d_{b1}^2} + \frac{\partial^2 S_2}{\partial d_{b2}^2} = V\left(\frac{\partial \mu_{b1}}{\partial d_{b1}} + \frac{\partial \mu_{b2}}{\partial d_{b2}}\right) \tag{22}$$

where we have introduced the number of cells V in each part of the lattice. Substituting the expressions for the chemical potentials, Eq. (10), into Eq. (22) gives

$$\partial^2 S/\partial d_{b1}^2 = -V\,(1/(1-\bar{d}_1) + 1/\bar{d}_{b1} + 1/(1-\bar{d}_2) + 1/\bar{d}_{b2}) \tag{23}$$

Introducing in addition to d_b the average total density

$$d = \tfrac{1}{2}(d_1 + d_2) \tag{24}$$

and using the equilibrium condition $\mu_{b1} = \mu_{b2}$, a straightforward calculation gives the fluctuation in terms of these nonfluctuating variables:

$$\delta^2 \Delta d = \frac{1}{V}\frac{16 d_b (1-d_r)(1-d)}{(2-d_r)^3} \tag{25}$$

In Fig. 3 the curves obtained from this expression are shown together with the corresponding values obtained from simulations. Again the

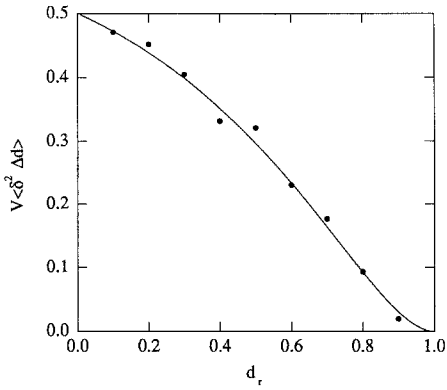

Fig. 3. The mean square fluctuation in the density difference $\langle \delta^2 \Delta d \rangle$ multiplied by the number of cells V in one of the lattices, as a function of the density of red d_r when $d_b = 1/2$. The dots give the simulation values obtained by time averaging over 20000 time steps.

exclusion principle is seen to play a dominating role: As $d_r \to 1$, the lattice is being filled up and the fluctuations are suppressed. The deviations from the curves obtained by theory seem to be solely a result of statistical uncertainties and decrease with increasing time averaging.

3. Osmotic Flow

Having examined the osmotic pressure in a system of fixed volume, we turn now to the analysis of the same system with fixed pressure. We consider the situation where there is no hydrostatic pressure difference across the membrane. The lattice gas will then mimic the flow from a reservoir of solvent into a reservoir of solution at the same pressure. We introduce a variable porosity ϕ, defined as the fraction of membrane sites being permeable to blue particles. The membrane is still impermeable to red particles. The results of the previous section, where we assumed $\phi = 1$, will still be valid in the case that $\phi \neq 1$ because they do not depend on the number of permeable sites.[2]

The boundary conditions, as seen by a color-blind observer, are periodic in all directions. But red particles leaving the right wall and entering the unmixed area are colored blue (the mixed area is now the right half of the lattice), while a specified fraction of the blue particles entering the mixed area are colored red. These boundary conditions ensure that there is no pressure difference across the membrane, and that there is a fixed concentration of red particles at the boundary of the mixed region. Initializing

[2] Changing ϕ in the previous context will be equivalent to changing the length of the membrane.

the system with a homogeneous mixture, there will be a flow of blue particles into the mixture, diluting it close to the membrane. Red particles will diffuse in the opposite direction of the flow, and, at steady state, the transport of red particles due to advection will equal the transport due to diffusion. Depending on the flow velocity, blue particles will receive a net momentum input from the membrane which is opposite and equal to the net momentum received by the red particles at steady state.

Before turning to the derivation of the steady-state current across the membrane, we need to describe the concentration boundary layer, i.e., the spatial dependence in the concentration of red particles. The site density of red particles $\rho_r(\mathbf{x}, t)$, defined as

$$\rho_r = \sum_{i=0}^{6} R_i \tag{26}$$

where $R_i = \langle r_i \rangle$ is the average occupation number in cell i, can be shown to obey the convection diffusion equation[2,17]

$$\frac{\partial \rho_r}{\partial t} + \mathbf{u} \cdot \nabla \rho_r = \nabla \cdot (D(\rho) \nabla \rho_r) \tag{27}$$

where D is the self-diffusion coefficient, ρ is the average uncolored site density

$$\rho = \sum_{i=0}^{6} N_i \tag{28}$$

and $\mathbf{u}$ is the average flow velocity defined through the relation

$$\rho \mathbf{u} = \sum_{i=0}^{6} \mathbf{c}_i N_i \tag{29}$$

$N_i = R_i + B_i$, where B_i is the average cell density of blue particles. In ref. 1 it is shown that the flow velocity $\mathbf{u}$ satifies the incompressible Navier–Stokes equation.

Equation (27) is derived by a Chapman–Enskog expansion in gradients[12] and relies on the assumption that the lattice gas may be set up with a separation between the time scale, the scale of spatial variations of ρ_r, and the lattice constant. It is also assumed that flow velocity u is small. Specifically, this means that when time is measured in units of simulation time steps and distance in units of the lattice constant, we have

$$\frac{\partial \rho_r}{\partial t} = o(\varepsilon^2) \tag{30}$$

$$\nabla \rho_r = o(\varepsilon) \tag{31}$$

$$u = o(\varepsilon) \tag{32}$$

where ε is a sufficiently small number. When we express mathematically the fact that the (average) number of red particles is conserved in both the collision and the propagation step, Eq. (27) results from a second-order expansion in ε. The diffusion coefficient $D(\rho)$ may be computed using the Boltzmann approximation, which assumes that particles entering a collision are uncorrelated. This has been done by several authors[2,17,18] for various choices of collision rules. We quote here the result obtained by d'Humières *et al.*[2]:

$$D = \frac{6}{7}\left(\frac{1}{1-\kappa} - \frac{1}{4}\right) \tag{33}$$

where

$$\kappa = 1 - 7d + \frac{35d^2}{3} - \frac{35d^3}{3} + 7d^4 - \frac{7d^5}{3} + \frac{d^6}{3} \tag{34}$$

and $d = \rho/7$ is the average cell density.

Integrating Eq. (27) over an arbitrary area of the lattice (regarding the densities and velocity as continuous functions being sampled at the nodes of the lattice), we obtain the mass current of red particles

$$J_r = \frac{2}{\sqrt{3}}(\rho_r \mathbf{u} - D\nabla\rho_r) \tag{35}$$

where the $2/\sqrt{3}$ factor is the inverse of the area per site of a hexagonal lattice.

At steady state the current of red particles vanishes:

$$\rho_r \mathbf{u} - D\nabla\rho_r = 0 \tag{36}$$

and we obtain a boundary layer of an exponential character:

$$\rho_r(x) = \rho_r(L)\, e^{(x-L)u/D} \tag{37}$$

where x is the distance measured from the membrane and L is the distance between the boundary and the membrane.

The mass transport j across a single membrane site, at position $\mathbf{x}$, during a time step is solely due to the transport of blue particles, and it can be written

$$j = \sum_{i=1,2} b_i(\mathbf{x}, t_+) - \sum_{i=4,5} b_i(\mathbf{x}, t_+) \tag{38}$$

when the lattice orientation is as shown in Fig. 1. The occupation numbers $b_i(\mathbf{x}, t_+) = 0$ or 1 are the number of blue particles in cell i *after* collisions. Expressing j by the precollision occupation numbers we find the interaction between the membrane and the gas,

$$j = \eta \left\{ \sum_{i=1,2} b_i(\mathbf{x}, t)[1 - n_{i+3}(\mathbf{x}, t)] - \sum_{i=4,5} b_i(\mathbf{x}, t)[1 - n_{i-3}(\mathbf{x}, t)] \right\} \tag{39}$$

Here $\eta = 1$ if the site is permeable to blue particles (open) and $\eta = 0$ if it is impermeable (closed). In the simulations η is chosen by generating a random number such that $\langle \eta \rangle = \phi$. The value of η will therefore be independent of the occupation numbers. We will also employ the Boltzmann approximation, i.e., assume that the precollision occupation numbers are statistically independent of each other, so that averages of products can be written as products of averages. Using this assumption and the fact that the flow must be perpendicular to the membrane, we find that the average mass current $J = \langle j \rangle$ across the membrane takes the form

$$J = 2\phi[B_1(1 - N_4) - B_4(1 - N_1)] \tag{40}$$

In steady state the net momentum input from the membrane must be zero since the flow encounters no other resistance than that from the membrane. This indicates that we can assume that the equilibrium distribution $N_i^{\text{eq}}(\rho, \mathbf{u})$ pertaining in the bulk of the gas also describes correctly the uncolored distribution close to and on the membrane. This assumption is not obvious, since the membrane collision rules do not satisfy semi-detailed balance, and it is *a priori* conceivable that there would be a density variation close to the membrane. The equilibrium distribution $N_i^{\text{eq}}(\rho, \mathbf{u})$ is a Fermi–Dirac distribution[12] which to first order in $\mathbf{u}$ can be written

$$N_i(d, \mathbf{u}) = d(1 + \tfrac{7}{3}\mathbf{u} \cdot \mathbf{c}_i) \tag{41}$$

As before, we shall denote the part of the lattice containing exclusively blue particles as part 1 and the part containing both colors as part 2. The uncolored distribution N_i is the same in both parts, whereas the colored distributions are not: While $B_1 = N_1$ on the membrane, since it describes a population of particles that are propagated from region 1, $B_4 = N_4 - R_4$ depends on the concentration of red particles in region 2. In this region R_i depends on the concentration gradient as well as the velocity. According to Eq. (32), these quantities are of first order in ε. To this order R_i takes the form

$$R_i = R_i^{\text{eq}} + \psi(\rho)(\mathbf{c}_i \cdot \nabla)\, \rho_r + o(\varepsilon^2) \tag{42}$$

where

$$R_i^{\text{eq}} = C_0 N_i^{\text{eq}} \tag{43}$$

and the form of the gradient correction follows from symmetry reasons: a combined rotation of $\pi/3$ of both $\mathbf{c}_i$ and $\nabla\rho_r$ must leave R_i invariant. The concentration C_0 is defined as

$$C_0 = \frac{\rho_r}{\rho} \tag{44}$$

where ρ_r and ρ are measured at $x = 0$. The factorized form of Eq. (43) is due to the completely random redistribution of color in the collision step. By performing the gradient expansion leading to Eq. (27), we can identify ψ through the relation

$$D = -(3\psi + \tfrac{3}{14}) \tag{45}$$

Also, since the number of blue particles is conserved everywhere and the mass current is due to the transport of blue particles alone, we have

$$J = \frac{2}{\sqrt{3}} \sum_{i=0,6} c_{ix} B_i = \frac{14}{\sqrt{3}} du \tag{46}$$

in both regions. Thus, using Eq. (36) to express $\nabla\rho_r$ by u and substituting u from Eq. (46) and ψ from Eq. (45) into Eq. (42), we obtain

$$R_i = C_0 \left(d + \frac{3J}{56D} \right) \tag{47}$$

when $i = 4$ or 5. Likewise, the uncolored distribution can be expressed by J as

$$N_i = d \pm \tfrac{1}{4} J \tag{48}$$

The strategy now is to substitute the distributions obtained as functions of J into Eq. (40) and solve for J. However, for practical purposes we express the result by the concentration $C_1 = C(\mathbf{x} = \mathbf{c}_1)$ next to the membrane rather than by $C_0 = C(0)$ which is assumed to be measured on the membrane. To first order in gradients we have

$$C_1 = C_0 + \frac{1}{\rho} (\mathbf{c}_i \cdot \nabla) \rho_r \tag{49}$$

which by Eq. (36) takes the form

$$C_1 = C_0 \left(1 + \frac{3J}{28dD} \right) \tag{50}$$

Substituting C_0 from Eq. (50) into Eq. (47), we can write everything on the right-hand side of Eq. (40) in terms of J, D, and ϕ and solve for J. Keeping only first-order terms in J, this gives

$$J = \kappa_o C_1 \tag{51}$$

where the osmotic permeability κ_o is given by

$$\kappa_o = \frac{4d(1-d)\,\phi}{2(1-\phi) + [d + (1-d)\,3/14D]\,\phi C_1} \tag{52}$$

It is seen that the permeability has a dependence on the concentration C_1. In simulations, however, the product ϕC_1 will always be small. The current will therefore receive only a small correction to linear behavior in C_1. It is also observed that the permeability increases with increasing diffusivity of the gas. This is not surprising, since the diffusivity affects the transport of red particles from the neighboring sites to the membrane.

A flow parallel to the membrane will be slowed down by the membrane collision rules since these give a 180 deg reflection for all but a fraction $(1-\phi)$ of the blue particles. This rule is known to give a nonslip boundary condition. Also, gradients in the velocity field will be of second order in ε. Thus, we expect that the above result will be valid to a good approximation even in this more general case.

The predicted current given in Eqs. (51) and (52) is obtained on the basis of the same assumption and properties of the gas as the transport equation (27). Both equations express the conservation of color in the gas; Eq. (27) is obtained directly from the local conservation law, and Eqs. (51) and (52) rely on the fact that the mass current of blue particles in the bulk of the gas is the same as the current on the membrane.

4. SIMULATIONS

The simulations were performed on a 40×100 lattice with an average cell density $d = 0.5$, and time averages were taken over 50,000 time steps. The concentration of red particles at the membrane was set indirectly by setting it at the boundary where it was varied from 0 to 1. As diffusion is the only mechanism of transport for the red solute particles, the lattice had to be small in the direction of the flow in order to get a sufficiently large concentration at the membrane. The size of the lattice still gives concentration gradients less than 0.05. The measurements shown in Fig. 4 confirm that the concentration boundary layer is indeed of an exponential character as predicted in Eq. (37). The plot shows $\ln[C(x)]/u$ as a function of the distance x from the membrane when the boundary concentrations

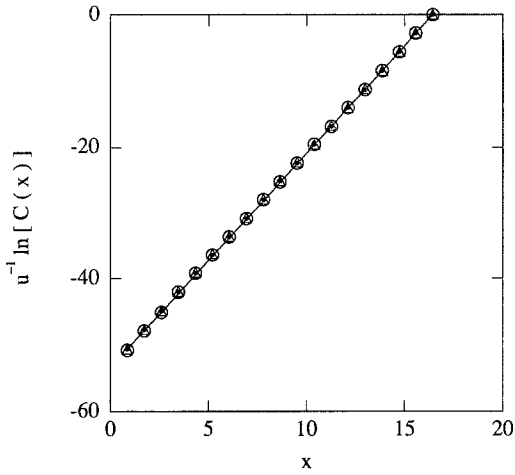

Fig. 4. The function $\ln[C(x)]/u$ as a function of x. The small dots correspond to the value of the porosity $\phi = 0.2$, the triangles to $\phi = 0.35$, and the larger circles to $\phi = 0.5$. The solid line is a straight line fit. The velocity u is obtained by measuring the mass current J, which is shown in Fig. 6, and using Eq. (46) to obtain u.

$C(L) = 1$. The velocity u is obtained by measuring the mass current J and using Eq. (46). The data corresponding to $\phi = 0.2$, 0.35, and 0.5 are collapsed on one curve, which by Eq. (37) has the slope $1/D$. The value of the diffusion coefficient $D = 0.290 \pm 0.004$ obtained by doing a straight-line fit of these data is within 2% of the Chapman–Enskog value calculated from Eq. (34),

$$D_{\mathrm{CE}} = 0.297 \tag{53}$$

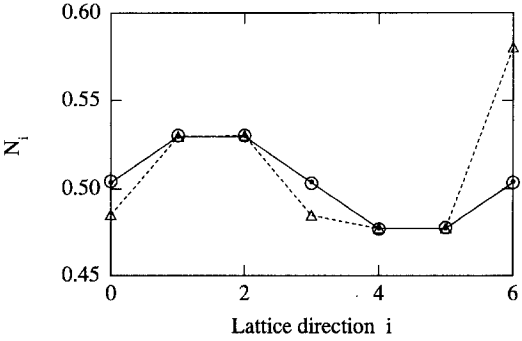

Fig. 5. The cell distribution function N_i as a function of the lattice directions, labeled with i, for the membrane sites and the two nearest neighboring sites. The membrane sites are represented by circles and the two neighboring rows are represented by triangles. The solid line is obtained from Eq. (41).

This shows that both the scale separation assumption and the Boltzmann approximation are reasonably good in the present context.

For a given input configuration to a collision there are in general several possible output configurations (35 at most) consistent with the conservation of the two colors and momentum. In the simulations the output

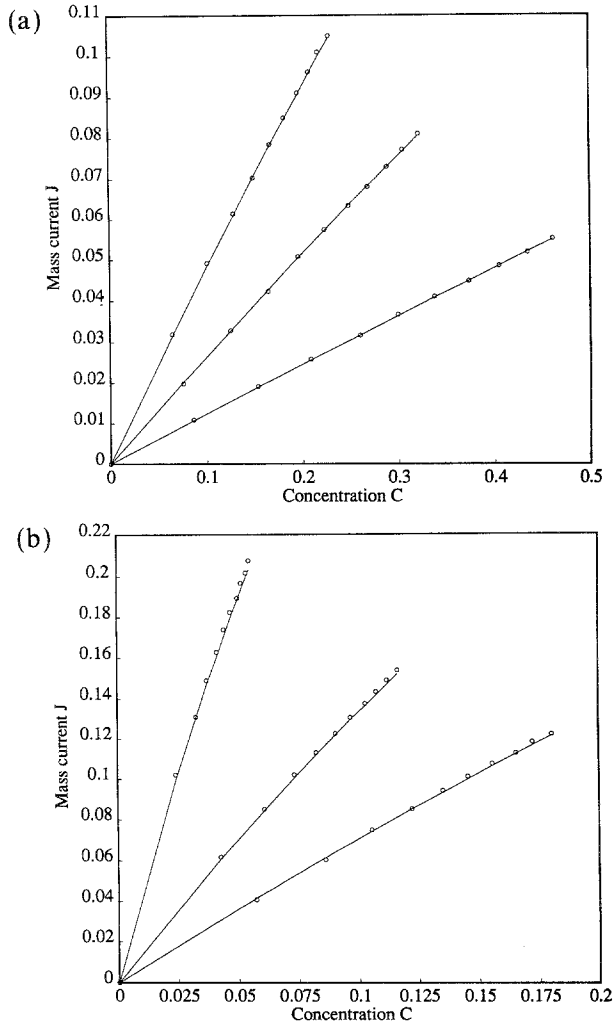

Fig. 6. The current of blue particles across the membrane $J = (14/\sqrt{3})\, du$ as a function of the concentration of red particles C_1 next to the membrane. The porosity ϕ ranges from 0.2 through 0.35 to 0.5 from bottom to top in (A) and from 0.6 through 0.75 to 0.9 from bottom to top in (B). Solid lines show the theoretical values given by Eqs. (51) and (52); the dots represent values obtained by simulations.

configurations were chosen in a stochastic manner using a quasi random number. For efficiency reasons we also attempted to select the output configurations by a counter variable which was increased by one for every site update. This procedure gives a deterministic lattice gas. It also gives a strongly nonergodic behavior. Periodic variations of the order 5% in the density profile $\rho(x)$ and characteristic steps in the concentration profile $C(x)$ did not vanish with increasing time averaging.

Figure 5 shows measurements of the cell distribution function N_i confirming that the Fermi–Dirac equilibrium indeed extends all the way to the membrane and that there are no variations in $\rho(x)$ close to the membrane. The solid line shows the theoretical values of N_i calculated from Eq. (41). The deviations from the equilibrium values of the populations in the cells 0, 3, and 6 on the membrane result because the membrane collision rules conserve the number of particles in these cells. The time-averaged density $\rho(x)$ shows spatial variations less than 0.001.

Figure 6 shows the mass current as a function of the concentration C_1 next to the membrane. The dots are results from the simulations, and the corresponding solid lines are obtained from Eqs. (51) and (52). The agreement is seen to be excellent for the values of the porosity $\phi = 0.2$, 0.35, and 0.5, where the simulation values are within 1% of the theoretical values. In this plot no systematic deviations are observed. For the porosities $\phi = 0.6, 0.75$, and 0.9 the theoretical curve is seen to lie slightly under the simulation values. This is most probably due to the corrections of second order in velocity and gradients that are not included in the expressions for the current (51) and (52). It is also seen that the current is very close to being linear in C_1, confirming that the product ϕC_1 is small.

5. CONCLUSION AND SUGGESTIONS FOR FURTHER APPLICATIONS OF THE MODEL

We have investigated the osmotic interaction across a semipermeable membrane at constant volume and constant pressure, respectively, using simple boundary conditions. We have shown that the model is well described by the theory introduced, both for the equilibrium pressure difference and for the nonequilibrium flow across the membrane. The model can be used to study a variety of more complicated systems with externally imposed flows and concentration gradients. From a biological point of view ot might be of particular interest to examine concentration boundary layers and the resulting osmotic flow in different hydrodynamic settings. Some analytic results due to Pedley[7,8] exist for stagnation point flow directed toward an infinite membrane and for flow parallel to a semi-infinite membrane. The derivations of these results are quite elaborate and

valid only in limited regimes. Other flows of interest are flows driven by an imposed difference in buoyancy between the different particle species and flows with external stirring. By introducing body forces close to the membrane, one might be able to mimic the combined effect of electrostatic and osmotic interactions known to exist over living cell membranes.

By introducing a position-dependent porosity, an inhomogeneous flow field will result. For low Reynolds number the transport of solvent toward the membrane will still be due to diffusion alone. But increasing the Reynolds number will lead to a transition to convection driven by the variations in the osmotic flow. Presumably this transition will be quite pronounced, since the convection will increase the concentration of solute at the membrane, thereby increasing the osmotic flow.

From the theoretical point of view the semipermeable membrane might be interesting as a statistical mechanical toy system. For instance, by extending the model to include nontrivial energy conservation and giving the membrane a specific heat conductivity, one could study the combined effects of concentration and temperature gradients. In this context one might be able to derive Onsager-type relations in a lattice gas.

ACKNOWLEDGMENTS

We thank A. Gunstensen, D. d'Humières, J. Somers, and E. Saugen for valuable comments and discussions. We gratefully achnowledge support by VISTA, a research cooperation between the Norwegian Academy of Science and Letters and Den norske stats oljeselskap a.s. (STATOIL), and by NAVF, the Norwegian Research Council for Science and the Humanities.

REFERENCES

1. U. Frisch, B. Hasslacher, and Y. Pomeau, Lattice gas automata for the Navier–Stokes equation, *Phys. Rev. Lett.* **56**:1505 (1986).
2. D. d'Humières, P. Lallemand, J. P. Boon, D. Dab, and A. Noullez, Fluid dynamics with lattice gases, in *Proceedings of Workshop on Chaos and Complexity*, R. Livi *et al.*, eds. (World Scientific, Singapore, 1988), p. 427.
3. D. H. Rothman and J. M. Keller, Immiscible cellular automaton fluids, *J. Stat. Phys.* **52**:1119–1127 (1988).
4. A. K. Gunstensen, D. H. Rothman, S. Zaleski, and G. Zanetti, A lattice-Boltzmann model of immiscible fluids, *Phys. Rev. A* **43**:4320–4327 (1991).
5. J. A. Somers and P. C. Rem, Analysis of surface tension in two-phase lattice gases, *Physica D* **47**:39–46 (1991).
6. U. Brosa, C. Kuttner, and U. Werner, Flow through a porous membrane simulated by cellular automata and by finite elements, *J. Stat. Phys.* **60**:875–887 (1990).

7. T. J. Pedley, The interaction between stirring and osmosis. Part 1, *J. Fluid Mech.* **101**:843–861 (1980).
8. T. J. Pedley, The interaction between stirring and osmosis. Part 2, *J. Fluid Mech.* **107**:281–296 (1981).
9. G. R. McNamara and G. Zanetti, Use of the Boltzmann equation to simulate lattice gas automata, *Phys. Rev. Lett.* **61**:2332 (1988).
10. F. J. Higuerra and S. Succi, Simulating the flow around a circular cylinder with a lattice Boltzmann equation, *Europhys. Lett.* **8**:517–521 (1989).
11. Y. H. Qian, D. d'Humieres, and P. Lallemand, Lattice BGK models for Navier Stokes equation, *Europhys. Lett.* **17**:479–484 (1992).
12. U. Frisch, D. d'Humieres, B. Hasslacher, P. Lallemand, Y. Pomeau, and J. P. Rivet, Lattice gas hydrodynamics in two and three dimensions, *Complex Systems* **1**:649–707 (1987).
13. D. d'Humieres, Y. H. Qian, and P. Lallemand, Invariants in lattice gas models, in *Proceedings of the Workshop on Discrete Kinetic Theory, Lattice Gas Dynamics and Foundations of Hydrodynamics*, I. S. I-R. Monaco, ed. (World Scientific, Singapore, 1988), pp. 102–113.
14. D. d'Humieres, Y. H. Qian, and P. Lallemand, Finding the linear invariants of lattice gas automata, in *Proceedings of the Workshop on Computational Physics and Cellular Automata*, A. Pires, D. P. Landau, and H. Herrmann, eds. (World Scientific, Singapore, 1989), pp. 97–115.
15. G. Zanetti, Hydrodynamics of lattice gas automata, *Phys. Rev. A* **40**:1539 (1989).
16. M. Hénon, An *H*-theorem for lattice gases, Appendix F in ref. 12.
17. C. Burges and S. Zaleski, Buoyant mixtures of cellular automata gases, *Complex Systems* **1**:31–50 (1987).
18. M. H. Ernst and T. Naitoh, Self-diffusion in CA fluids, *J. Phys. A: Math. Gen.* **24**:2555–2564 (1991).